ORIGINAL CONTRIBUTION

Synthesis of Ag nanoparticles by cathode glow discharge electrolysis using sacrificial Ag foil of anode

Quanfang Lu[1,2] · Xiaojuan Ma[1] · Jie Yu[1] · Bo Wang[1] · Yan Feng[1] · Xiaoxia Hao[1] · Yuheng Qian[1] · Qingying Ma[1]

Abstract

Silver nanoparticles (Ag NPs) were prepared in Na_2SO_4 solution with adding ethanol via cathode glow discharge electrolysis (CGDE) plasma using sacrificial anode as a source of Ag^+ ions, in which Ag foil and Pt needle were served as anode and cathode, respectively. The physical characteristic of CGDE was investigated by current-voltage curve and oscilloscope. Ag NPs were characterized by XRD, UV-Vis, SEM/EDX, TEM and XPS. The preparation mechanism was discussed. The results showed that at 520–620 V discharge, the high energetic electrons impact water at plasma-liquid interface to form many active species, i.e., H●, O●, OH●, e_{aq}^-, OH^- and H_2O_2. Adding 15 mL ethanol into the 150 mL electrolyte can trap oxidizing agent OH● and suppress producing $AgOH/Ag_2O$. High purity Ag NPs are fabricated via the reduction of Ag^+ ions by e_{aq}^- and H● in plasma cathode. Compared with other plasma-liquid interface technique, CGDE offers a simple, fast, high effective and environment friendly method for the synthesis of Ag NPs.

Introduction

Noble metal (Ag, Au, Pt, Pb) nanoparticles (NPs) have been studied extensively because of their unique properties compared with bulk materials, such as catalytic, electric, magnetic, optical and mechanical properties [1]. Among them, silver NPs (Ag NPs) have actually got expansive attention because of the engaging optoelectronic properties, awesome antibacterial capabilities, and plasmon resonance in the visible range [2, 3]. Various approaches have been reported for the preparation of Ag NPs with desirable size, such as biological, photochemical, physical, and chemical methods [4, 5]. Each method has different advantages and issues, such as cost, particle size, size distribution and scalability [6]. Among them, chemical reduction is the most popular preparation method for Ag NPs. However, during the process of chemical synthesis, many factors such as reducing agent, temperature, solution pH, surfactant and dispersing agent can greatly affect the quality and quantity of Ag NPs, and ultimately influence the property and application. In addition, most chemical approaches often use many toxic and expensive chemicals which cause environmentally harmful [7]. Since Ag NPs are widely applied in a variety of situations of our daily life, developing an easy, economical and eco-friendly preparation method is currently the focus of most attention.

In recent years, plasma-liquid interactions at atmospheric pressure have received great attention as a prominent "green" synthesis strategy for Ag NPs due to its low operating costs, mild reaction condition, rapid synthesis, high effectiveness, and environmental friendliness [8, 9]. Their use in nanomaterials preparation only depends on production of various active species, such as hydrated electrons (e_{aq}^-), H●, O●, OH●, OH^- and H_2O_2, and other phenomena occurring at plasma-liquid interface and being responsible for reducing the metallic precursors [10, 11]. The addition of reducing agents in plasma-liquid systems is no need at all. Moreover, the whole nanomaterial preparation has been found to be simple, rapid and clean [12]. Therefore,

✉ Quanfang Lu
luqf@nwnu.edu.cn

✉ Jie Yu
yujie741008@163.com

[1] College of Chemistry and Chemical Engineering, Northwest Normal University, Lanzhou 730070, China

[2] Editorial Department of the University Journal, Northwest Normal University, Lanzhou 730070, China

many groups have recently reported for the generation of Ag NPs using plasma-liquid systems [13–22]. For example, Richmonds and Sankaran [15] first developed an atmospheric pressure direct current (dc) argon plasma jet (acted as cathode) being in contact with a dilute acid solution for the synthesis of Ag NPs in which an Ag foil was immersed into the solution (acted as anode), and fructose was used as stabilizer to prevent the aggregation of Ag NPs. They believe that Ag NPs are prepared through plasma-injected electrons to directly reduce the Ag^+ ions in solution. Then, Shirai et al. [16] proposed dual atmospheric glow discharge helium plasma jets as electrodes in a Hofmann electrolysis apparatus to prepare the Ag NPs, in which $AgNO_3$ solution was acted as precursor of Ag NPs. They found that Ag NPs were only produced on the plasma cathode region via the reduction of Ag^+ by electrons, and positive ion and electron irradiation from the plasma produces H^+ and OH^-, respectively, in the solution. After that, to make the Ag NPs disperse well, sucrose [17], fructose [18] and dextran [19] were added into the $AgNO_3$ solution as stabilizer agent for the preparation of Ag NPs by atmospheric pressure dc He and/or Ar microplasma. However, these methods consume a lot of noble gases, the utilization of plasma is not high at jets of the solution surface, the reaction rate is uncontrollable, and the experimental setup is complex. In addition, the size and dispersion of the Ag NPs can also be controlled by pH and temperature [18, 20]. Moreover, the use of $AgNO_3$ solution makes difficult the control of size and shape of NPs due to the change of metallic ions concentration in the working solution [17–19]. Recently, Kuntyi et al. [21] found that Ag NPs were prepared by contact glow discharge microplasma with "sacrificial" Ag foil anode, in which polyvinylpyrrolidone (PVP) is used as a stabilizer, and NaOH and sodium acetate (NaAc) were used to adjust the pH = 8. However, stabilizer PVP is a toxic chemical, which will limit the application of Ag NPs. Moreover, the production rate and size of Ag NPS depends on the nature of regulating agent NaOH or CH_3COONa. Therefore, the preparation process is very complex. Shepida et al. [22] reported that the stabilized Ag NPs were formed in solutions of the sodium polyacrylate (NaPA) and $AgNO_3$ by tungsten cathode plasma glow discharge. However, the pH value of the solutions was adjusted with CH_3COONa to 8. Based on the above examples, although many preparation techniques of Ag NPs using plasma-liquid systems have been reported [17–22], the details of preparation mechanism and generation of size-controllable Ag NPs are still limited due to the lack of understanding of plasma-liquid interactions.

Glow discharge electrolysis (GDE), also called as contact glow discharge electrolysis (CGDE) and/or plasma electrolysis (PE) [9, 23, 24] is a novel kind of electrochemical process where the plasma is sustained in liquid by direct-current glow discharge between a pointed electrode (either at the anode or at the cathode, when the plasma is generated in liquid around cathode, it is called cathode glow discharge electrolysis (CGDE), and vice versa) and the electrolyte around it [25, 26]. If the applied voltage is sufficiently high in aqueous media, the conventional electrolysis is spontaneously converted into glow discharge electrolysis. In this case, the charge transfer, high electric field, ultraviolet light, ultrasound, electrohydraulic cavitation, as well as even shock wave are generated around one of the electrodes immersed in the electrolyte. Meanwhile, a variety of reactive species such as e_{aq}^-, $H^\cdot$, $O^\cdot$, $HO^\cdot$ and H_2O_2 are formed which can promptly diffuse into the solution to induce some unimaginable chemical reactions [25–27]. Over the past 20 years, GDE has been widely applied in water treatment [28], hydrogen generation [29], surface modification [30], synthetic chemistry [31] and analytical chemistry [32]. However, it is few reported for the preparation of NPs [33]. Recently, TiO_2 NPs [34] and β-Ni(OH)$_2$ microsphere [35] can be efficiently produced by a one-step method via cathode glow discharge electrolysis (CGDE) plasma technique in liquid. The results indicated that the CGDE can be regarded as a novel green technique for the preparation of NPs from bulk material. However, the physical characteristic of plasma and preparation mechanism need further study.

Herein, Ag NPs were successfully synthesized in the electrolyte of 2 g L^{-1} Na_2SO_4 with adding ethanol by CGDE technique, in which Pt needle and Ag foil (as precursor of Ag NPs) were acted as cathode and anode, respectively. The physical characteristic of CGDE was investigated by current-voltage curve and oscilloscope. The component, structure and morphology of Ag NPs were analyzed by X-ray diffraction (XRD), UV-Vis spectroscopy, scanning electron microscope (SEM), transmission electron microscopy (TEM) and X-ray photoelectron spectroscopy (XPS). The emission spectra of CGDE were determined by optical fiber spectrometer, and the preparation mechanism was also discussed in detail.

Experimental section

Experimental materials

Na_2SO_4 and ethanol were of analytical grade and supplied by Shanghai Chemical Reagent Co. LTD, China. Methyl orange and phenolphthalein used as pH indicators were of analytical grade and provided by Kameshu Biotechnology Co., LTD, China. Silver foil (> 99.99%) as precursor of Ag NPs was purchased from Qinghe County Jinjia Metal Material Co. Ltd., China. A homemade Pt needle (diameter: 0.5 mm) was sealed into a quartz tube and kept a 1.0 mm distance from the top of the quartz tube. Pt needle was used as cathode

materials due to its high melting point, acid-proof, alkali-proof and corrosion resistance.

Synthesis of Ag NPs by CGDE

The experimental setup for the preparation of Ag NPs was presented in Fig. 1a. The reactor was a 200 mL quartz vessel equipped with a silver foil anode and a Pt needle cathode. The 150 mL of 2 g L^{-1} Na$_2$SO$_4$ was used as the electrolyte and adding a certain amount of ethanol was employed as capture agent of OH●. A DH1722A-6 high-voltage dc power supply purchased from Beijing Dahua Radio Instrument Factory of China was applied to sustain the discharge at the constant-voltage mode. The date of voltage and current were obtained by built-in high-precision ammeter and voltmeter, respectively. A 2 kΩ resistor was connected in the circuit to stabilize and limit the current. The Ag foil was placed parallel to the Pt needle with a 5 mm gap between them. During the experiments, the solution was stirred at 120 r min^{-1} by a magnetic stirrer, and the solution pH and conductivity were measured using pH meter and conductivity meter, respectively. When the voltage was over 520 V, the glow was generated around the Pt needle of the cathode, and the produced gas such as O$_2$ and H$_2$ was expelled from the gas outlet. The discharge was lasted for 30 min at 25 °C, the colour changes of solution are shown in Fig. 1b, and the brown products were formed in the solution. After that, the produces were collected by centrifugation at 8000 r min^{-1}, washed with distilled water several times, and dried at 60 ℃.

Measurement of solution pH values around cathode and anode

The setup for the measurement of pH values around cathode and anode is described as follows. The Pt needle and Ag foil were placed in two glass tubes, and the gap between the two glass tubes was about 5 mm. The indicators such as methyl orange and phenolphthalein were dropped into the glass tubes, and then the color changes were observed during the process of discharge [34, 35]. In addition, the solution pH and conductivity around anode Ag foil and cathode Pt needle were also measured by pH meter and conductivity meter, respectively.

Characterization of Ag NPs

Voltage and current waveforms of the CGDE were recorded on an oscilloscope of Tektronix TDS3052C. The phase

Fig. 1 **a** The experimental setup of CGDE for the preparation of Ag NPs, and **b** colour changes of products at 520 V in 2 g L^{-1} Na$_2$SO$_4$ solution with 15 mL ethanol
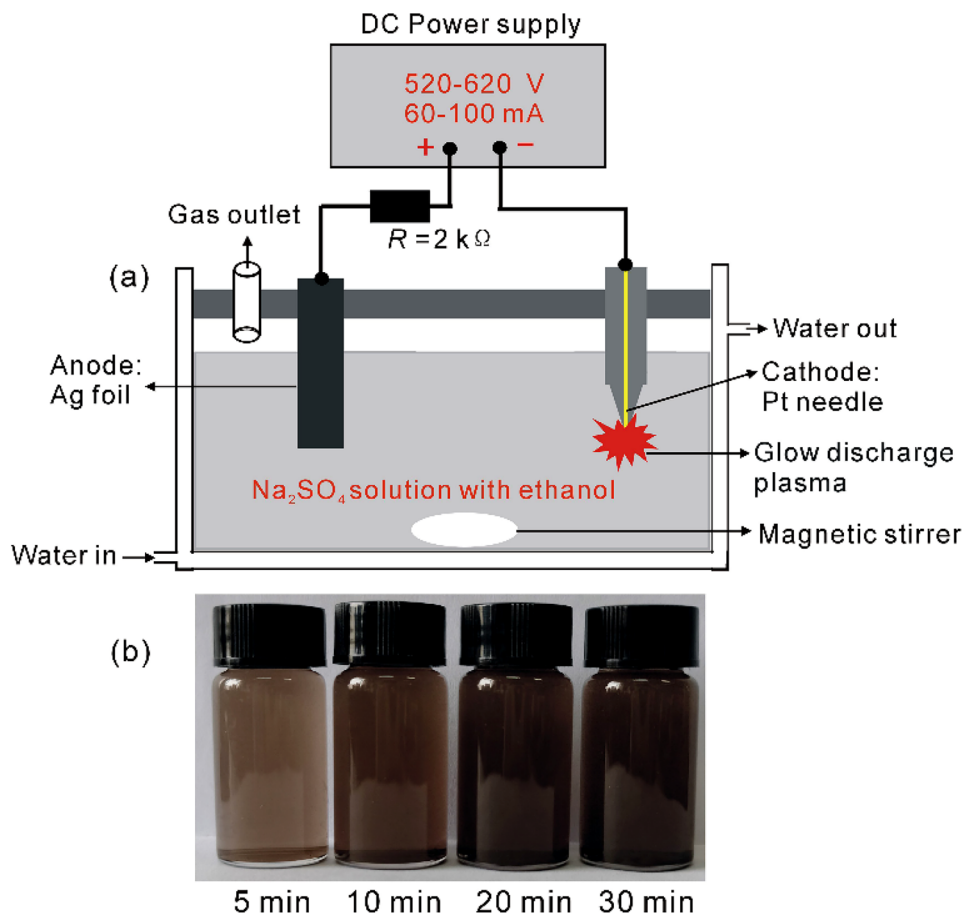
composition and crystalline structure of products were identified by a powder X-ray diffraction (XRD, D/Max-2400, Rigaku) with Cu-K$_\alpha$ radiation ranging from 5° to 80°. UV-vis were performed on an UV757CRT Ver 2.00 (Shanghai Keheng Instrument Factory, Shanghai). Morphologies were observed by scanning electron microscope (SEM, JSM-5600 LV) and high-resolution transmission electron microscope (TEM, JEM-2100 plus). X-ray photoelectron spectroscopy (XPS) tests were performed using Thermo Scientific ESCALAB 250Xi equipped with Al-K$_\alpha$ X-rays as the excitation source. The emission spectrum of CGDE was recorded on an optical fiber spectrometer (AvaSpec-ULS2048-8-USB2).

Results and discussion

Typical current-voltage behavior

At present, many issues about the mechanisms of glow discharge electrolysis plasma are still unclear [36]. In order to understand the discharge mechanism, the typical current-voltage characteristics in 150 mL 2 g L^{-1} Na$_2$SO$_4$ solution with adding 15 mL ethanol are presented in Fig. 2a (The error bars represented the combined error from the three measurements). Several regions are usually identified [26, 37, 38]:

- $0 < V < V_B$: 0–490 V, Ohmic region. The current increases linearly with the increase of voltage according to Ohmic law [26, 37, 38]. Conventional electrolysis of water takes place with small gas bubbles leaving the pointed cathode.
- V_B: 490 V, breakdown voltage. Joule heating (IR loss) is concentrated at the cathode-solution interface, the solution surrounding the point cathode is heated to the boiling point and a gas bubbles including water vapor and hydrogen gas are produced [39, 40]. In this point, small flashes of light resulting from gas breakdown are generated. The electric field between the cathode and the positive charges on the sheath results in the electric breakdown of the vapor bubbles.
- $V_B < V < V_C$: 490–520 V, unstable region or transition region. Joule heating leads to local vaporization of water adjacent to the Pt needle cathode, and subsequently the continuous pulsating vapor sheath is formed surrounding the cathode Pt wire which isolates the cathode surface from the electrolyte solution [38]. The formation of the vapor sheath due to localized heat is a key factor because the ignition condition is determined by the thickness of a sheath and the gas pressure, that is, Paschen's law [38]. In this region, the surface of the immersed Pt needle electrode is covered by an unstable vapor sheath, which intermittently blocks the current [41]. Therefore, the fluctuation of the current occurs. Meanwhile, the current starts
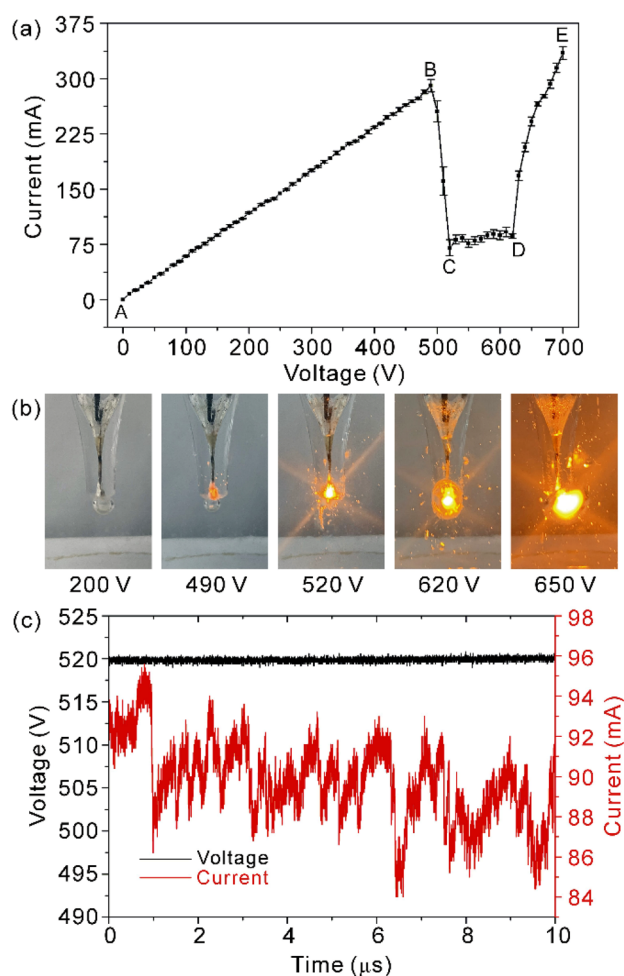

Fig. 2 **a** The typical current-voltage characteristics curve during the process of CGDE, **b** photographs at different applied voltage, and **c** the voltage and current waveforms of the CGDE at 520 V in 2 g L^{-1} Na$_2$SO$_4$ solution with 15 mL ethanol

to decrease with the applied voltage. This is because the conductivity of the vapor sheath is lower than that of the solution, and the equivalent electrical resistance of the vapor sheath is much higher than that of the electrolyte, which lead to a sudden decrease in the current [26]. In addition, the majority of the voltage across the cell drops over the vapor sheath inducing a high electric field [26].

- V_C, 520 V, critical voltage or midpoint voltage. The current falls sharply to a lower value, and the gaseous sheath around the cathode slowly stabilizes. Therefore, V_C is the threshold level of glow discharge.
- $V_C < V \leq V_D$: 520–620 V, normal glow discharge region. In this region, the vapor sheath forms a glow discharge plasma, and the current is transported through glow discharge plasma. The electronically excited atoms drop down immediately to a stable energy level by emitting unique photons as visible light [38]. However, the current slowly start to increase again with increasing the

voltage in this region. This is because the vapor sheath in the cathode region at high voltage operation is almost saturated by the excessive evaporation [42].

- $> V_D: > 620$ V, abnormal glow discharge region. With increasing the applied voltage, the current begins to increase promptly because of the high conductivity of the plasma [35]. However, beyond point D, the Pt electrode becomes red hot, and further increase the voltage can lead to melting and damage of Pt electrode due to too excessive Joule heating under high power.

Based on above analysis, the glow discharge is believed to form through local Joule heating of the solvent near the electrode surface that vaporizes and subsequently breaks down at high electric fields, and then the electronically excited atoms drop down immediately to a stable energy level by emitting unique photons as visible light.

Figure 2b illustrates the photographs around Pt needle electrode during the discharge process. Photographs of 200, 490, 520, 620 and 650 V represent the Ohmic region, breakdown voltage, critical voltage, strong glow discharge and abnormal glow discharge, respectively. It is observed that when voltage is sufficiently high, a glow discharge with intense light emission starts in the gas sheath around the Pt cathode and the light emission area expands with further increasing the voltage. This observation is in good agreement with the reported by Toriyabe et al. [38]. Since the excitation energies are characteristic for atom species, the color of the emitted light depends on the electrolytes [38]. Herein, the color of the light emission is yellow because of the characteristic of the Na atomic emission line in the presence of Na_2SO_4 [34, 35].

In order to further clarify the electrical characteristics of the plasma, the voltage and current waveforms of the CGDE at 520 V in 2 g L^{-1} Na_2SO_4 solution with 15 mL ethanol were recorded on oscilloscope. As can be seen from Fig. 2c, at 520 V applied voltage, the voltage remains a constant while current is a variable in the range from 84 to 96 mA. The fluctuation of the current takes place probably due to the commonality of discharge plasmas [36].

The structure, component and morphology analysis

X-ray diffraction (XRD) analysis

The component, phase and crystallinity of products under the different amounts of ethanol were investigated using XRD. As displayed in Fig. 3a, the product in 150 mL 2 g L^{-1} Na_2SO_4 without adding ethanol is a mixture of Ag_2O and Ag. The diffraction peaks at $2\theta = 32.79°$, 54.90°, 65.44° and 68.75° are assigned to the characteristics of Ag_2O, which are identified as the (111), (220), (311) and (222) crystal planes of Ag_2O (JCPDF 41–1104) [43]. The diffraction
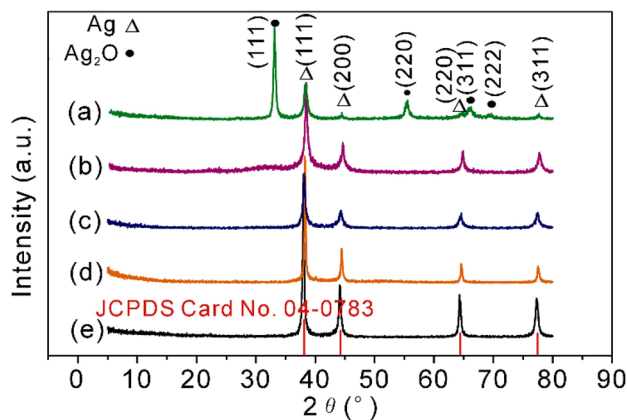

Fig. 3 XRD patterns of products at 520 V in 150 mL 2 g L^{-1} Na_2SO_4 with adding different ethanol content: **a** 0 mL, **b** 5 mL, **c** 10 mL, **d** 15 mL, and **e** 20 mL

peaks at $2\theta = 38.12°$, 44.28°, 64.43° and 77.47° are corresponded to the (111), (200), (220) and (311) crystal planes with face-centered cubic (fcc) structure of Ag (JCPDS No. 04–0783) [44]. With the increase of ethanol from 0 to 20 mL (Fig. 3a–e), the diffraction peaks of Ag_2O gradually disappear, indicating that the products are gradually transformed into Ag. After adding 15 mL ethanol, no other peaks of Ag_2O are detected, the purity of Ag is more than 95%. This is because adding ethanol into the liquid can change the composition of plasma, trap oxidizing agent (OH•) and suppress producing Ag_2O [45]. Therefore, the optimum amount of ethanol was 15 mL.

In addition, the sharp peaks of the XRD pattern (Fig. 3d, e) indicated that the synthesized Ag particles are well crystalline, and the broadening of peaks shows nanometer range of Ag particles [46–48]. Moreover, the particularly high peak intensity at 38.12° suggests that the Ag NPs have a preferential growth on the (111) crystal plane [49]. The average crystallite size was estimated by Scherrer's formula [35]:

$$D = \frac{k\lambda}{\beta \cos \theta} \tag{1}$$

Based on Scherrer's formula, the (111), (220) and (311) crystal planes were used to calculate the average size of the crystallites. The result found that the average crystallite size of the products at 520 V (Fig. 3d) is about 25 nm.

UV-vis spectroscopy analysis

UV-Vis spectral is a basic and simple approach for characterizing Ag NPs [2, 9]. This is because the λ_{max} of the localized surface plasmon resonance (LSPR) absorption band for Ag NPs is situated in the range of 400–750 nm [10]. As shown in Fig. 4a, the λ_{max} of the LSPR absorption
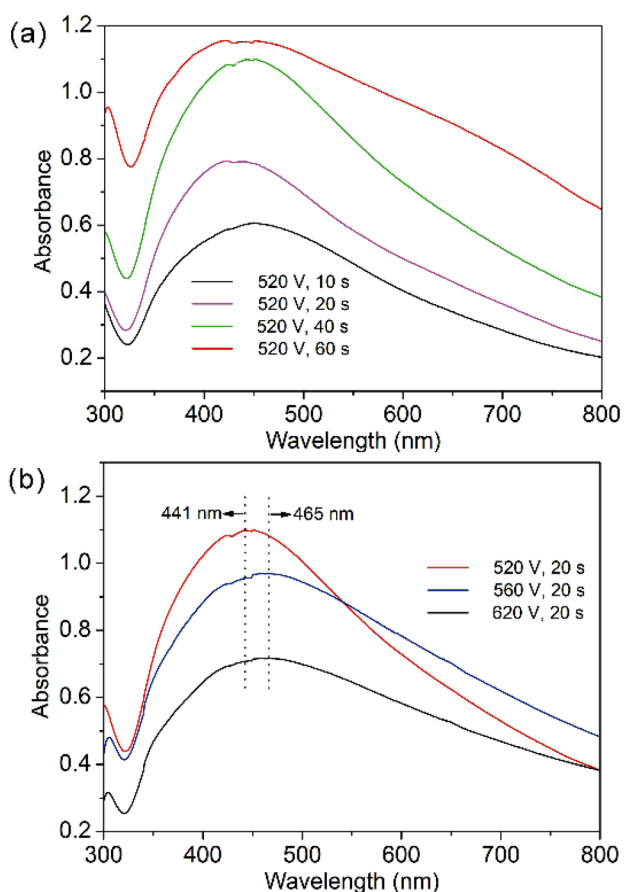
Fig. 4 UV-Vis spectra of Ag NPs in 150 mL 2 g L^{-1} Na_2SO_4 with adding 15 mL ethanol: **a** various discharge times from 10 to 60 s at 520 V, and **b** various voltages from 520 to 620 V in 20 s

presented in Fig. 4b. Increasing of the λ_{max} and broadening of the surface plasmon resonance band of Ag NPs are due to the wide size distribution of the obtained nanostructures and/or aggregation of Ag NPs [10]. The result that the size distribution of Ag NPs is increased significantly as increasing the discharge voltage is in accordance with reported by Jin et al. [44].

SEM/EDX analysis

The morphology and microstructure of as-prepared Ag NPs at 520 V (a), 560 V (b) and 620 V (c) were analyzed by SEM. As shown in Fig. 5a, Ag NPs have slight agglomeration and particle sizes are about 20–80 nm at 520 V. With the increase of the discharge voltage, the agglomeration of nanoparticles is gradually serious and the particle size is increased (Fig. 5b, c), indicating that higher discharge voltage is not conducive to the synthesis of small size Ag NPs. This change of morphologies could be attributed to the strong plasma reaction [44, 50]. Therefore, 520 V applied voltage was selected as the best discharge voltage.

The elemental compositions and purity of Ag NPs (Fig. 6a) were also analyzed by energy dispersive X-ray spectroscopy (EDX) and elemental mapping analysis. Elemental mapping image (Fig. 6b) confirms the existence and homogeneously distribution of Ag elements in the NPs. The EDX spectrum of Ag NPs (Fig. 6c) contains only Ag and C elements, and the atomic percentage of Ag and C element is about 83.9% and 16.1%, respectively, indicating the silver (Ag) are the major component of synthesized particles. The presence of C as shown in Fig. 6c can be attributed to the sample copper grid used for the analysis and/or the chemical compositions of the ethanol [51, 52]. These results exposed that the as-prepared Ag NPs have no impurity of Ag_2O. This result is in good agreement with the XRD analysis (Fig. 3d).
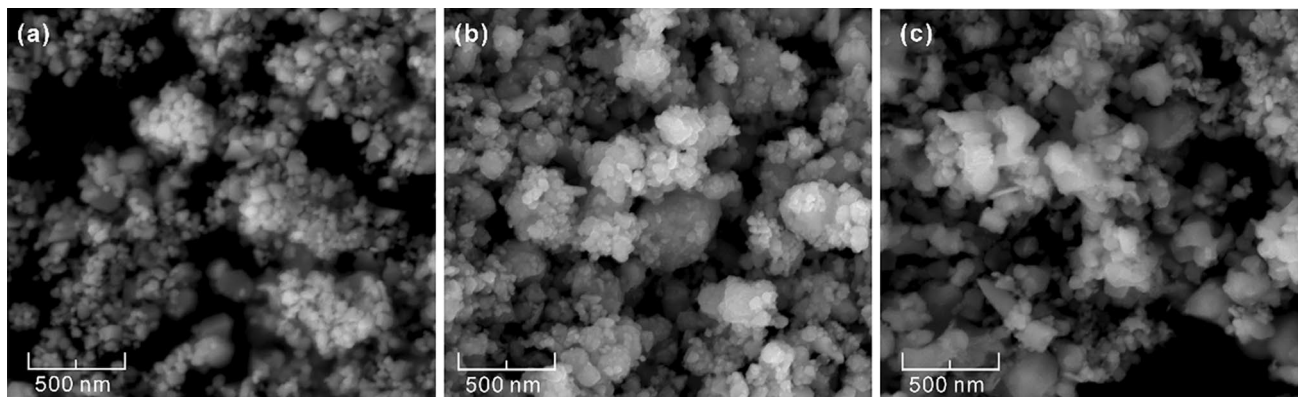
band was observed at about 441 nm. The results suggested that the Ag NPs can be prepared by using CGDE. With the increase of discharge voltage from 520 to 620 V (Fig. 4b), the λ_{max} of Ag NPs shifts from 441 to 465 nm, and the maximum absorbance intensity gradually decreased, as

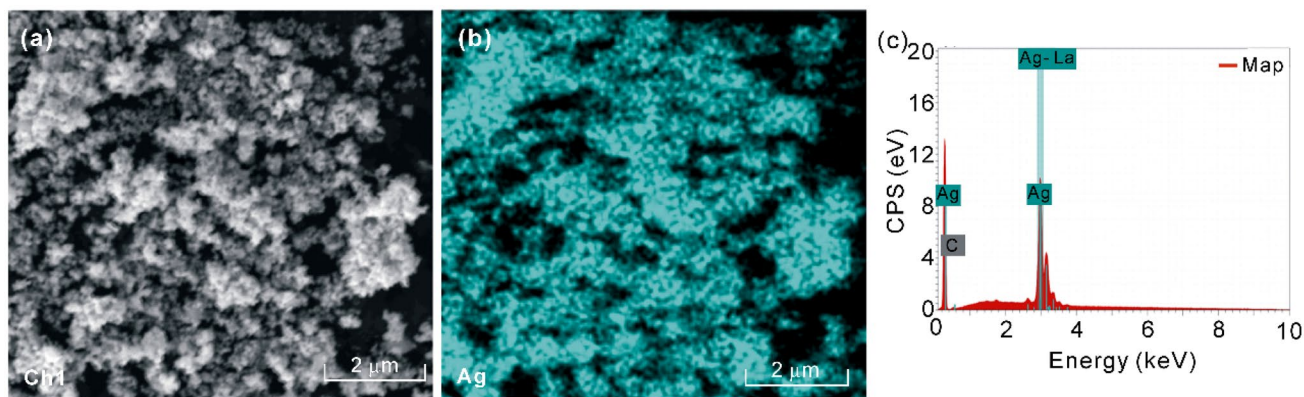**Fig. 5** SEM image of the Ag NPs prepared in 2 g L^{-1} Na_2SO_4 solution with 15 mL ethanol at **a** 520 V, **b** 560 V and **c** 620 V

Fig. 6 The elemental composition of Ag NPs prepared in 2 g L^{-1} Na_2SO_4 solution with 15 mL ethanol at 520 V: **a** SEM image, **b** elemental mapping, and **c** EDX elemental profile

TEM analysis

TEM was also utilized to observe the structure of Ag NPs with various discharge voltage. As shown in Fig. 7, the particle size of a (520 V) is much smaller than that of b (560 V) and c (620 V). Moreover, b and c show a certain aggregation. It further revealed that the average particle size of the Ag NPs is increased as the voltage increased, and the high discharge voltage is not conducive to the synthesis of Ag NPs. This is because the higher the voltage, the more excitation energy and atomization efficiency of Ag are increased, which can produce more active particles, lead to quite quickly reaction rate and impede the growth of regular orientation and order array [44, 50].

At HR-TEM image (inserted in Fig. 7a–c), the adjacent lattice fringe is estimated and found to be 0.2301, 0.2297 and 0.2354 nm, respectively, which is in proximity to the lattice spacing of (111) plane of fcc phase Ag (0.2340 nm) [44]. The selected area electron diffraction (SAED) pattern shows the different intensities of bright rings as illustrated
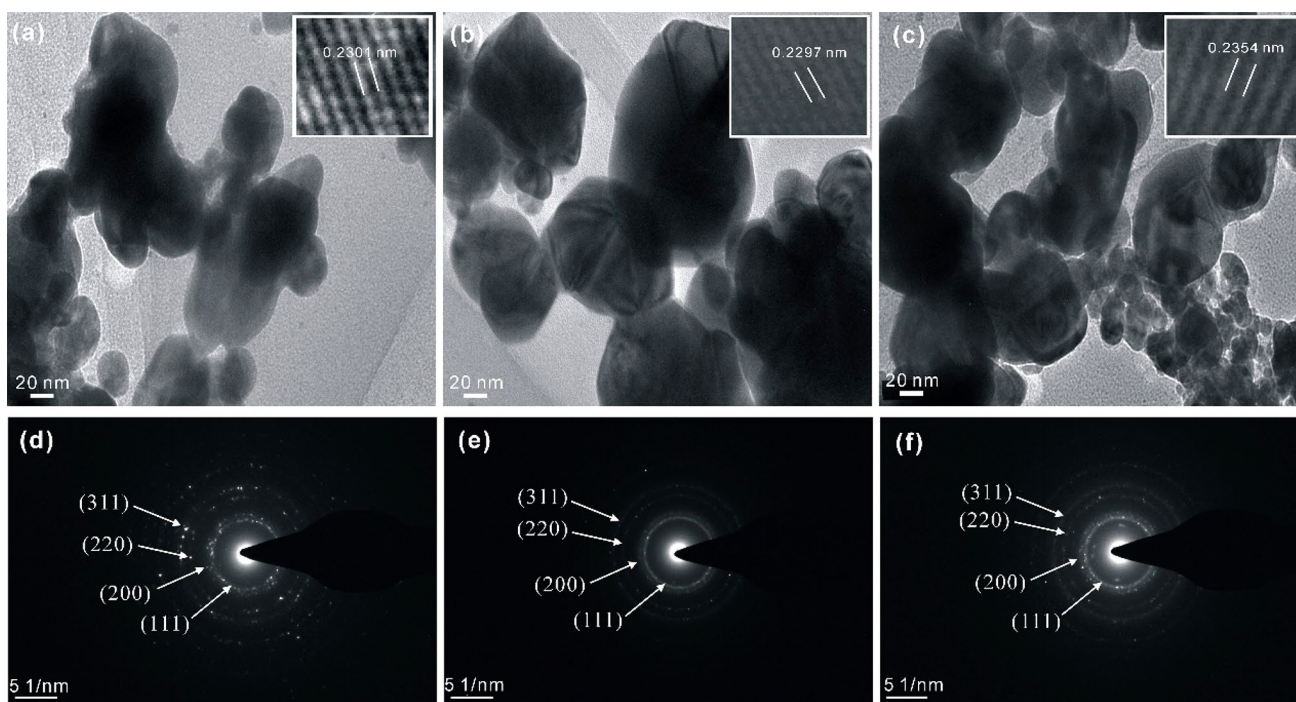

Fig. 7 TEM images (**a** 520 V, **b** 560 V and **c** 620 V) and SAED patterns (**d** 520 V, **e** 560 V and **f** 620 V) of the Ag NPs prepared in 2 g L^{-1} Na_2SO_4 solution with 15 mL ethanol

in Fig. 7d–f, indicating it is highly crystallized. On the basis of the SAED pattern, the *d*-spacings are calculated to be about 0.2334, 0.2083, 0.1452, and 0.1350 nm, which correspond to (111), (200), (220), and (311) crystal planes of fcc crystalline structure of Ag [2]. The result of SAED and lattice fringes are consistent with the results from the XRD pattern (Fig. 3d) and UV-Vis spectral (Fig. 4b).

XPS analysis

X-ray photoelectron spectroscopy (XPS) is widely used to characterize elemental valence states and composition of metal nanoparticles [53]. Thus, the Ag NPs was examined by XPS. The survey spectrum of XPS is shown in Fig. 8a. The chemical binding energies located at 284.8, 531.1, 368.5, 573.9, and 604.6 eV are attributed to the characteristic peaks of C 1s, O 1s, Ag 3d, Ag $3p_{5/2}$ and Ag $3p_{3/2}$, respectively. The strong Ag signal peak at about 368.3 eV demonstrates the emergence of the Ag element [54]. The binding energies of the XPS spectra were calibrated by C1s (284.8 eV).

Figure 8b shows the Ag 3d fine spectra. Two peaks at 374.4 and 368.4 eV are corresponded to the binding energies of Ag $3d_{3/2}$ and Ag $3d_{5/2}$, with a spin energy separation of 6.0 eV, which is in good agreement with the spin–orbit splitting value of signature of Ag^0 species [55]. This result further offers a certain proof that the nanoparticles are indeed existed in zero valent state of Ag^0 and confirms reduction of Ag^+ to Ag^0 by the CGDE.

From Fig. 8c, the high resolution O 1s XPS spectrum is deconvoluted into two peaks that are centred at 532.6 and 531.4 eV, which cause by the surface absorbed H_2O and O_2. The high binding energy component at 532.6 eV is related to metal-OH bonds or H_2O adsorbed on surface of Ag NPs, and a small component at 531.4 eV is usually assigned to the subsurface O bonding of absorbed oxygen [56].

Discussion for the formation mechanism of Ag NPs

Spectral characteristics of CGDE

To discuss the formation mechanism of Ag NPs, optical emission spectra were recorded on optical fiber spectrometer. As illustrated in Fig. 9a, the lines at 283.0–309.0 nm are assigned to OH bands, and atomic lines attributed to H (H_α at 656.3 nm) and O (844.6 and 777.1 nm) are observed, which are produced when the water vapor in the plasma cathode is bombarded by high energy electrons [35]. In addition, the strong Ag atomic lines are also observed at 328.1 and 338.3 nm, suggesting that Ag atoms appear and Ag NPs are formed in the plasma-liquid region [3, 57]. Moreover, because the discharge is carried out in Na_2SO_4 solution, the Na atomic lines are also observed at 589.0 and 819.4 nm [32]. Based on the emission spectral of CGDE, it is found that active species, such as •H, •O and •OH are generated. In addition, H_2O_2 and e_{aq}^- are also produced during the process of CGDE. Among the active species, e_{aq}^- and H• are extremely reactive species with a reduction potential of –2.87 and –2.30 V, respectively, and HO˙ and H_2O_2 are strong oxidants with the standard potential of 2.85 and 1.76 V [8]. Therefore, CGDE is widely used in oxidation reaction [37], reduction reaction [29], addition reaction [31], and spectral analysis [32].

Calculation of plasma parameters

The plasma parameters, i.e., rotation temperature (T_{rot}, K) and electron density (N_e, cm^{-3}) are both important parameters for in depth understanding the preparation mechanism [58]. The Lifbase [59] computer programs are often applied to simulate the emission spectra of OH (A–X) band for rotational temperature in plasma electrolysis. In the process of simulation, the emission spectral data of OH in the range of 305–320 nm were selected, and Lifbase software was used to fit the experimental data
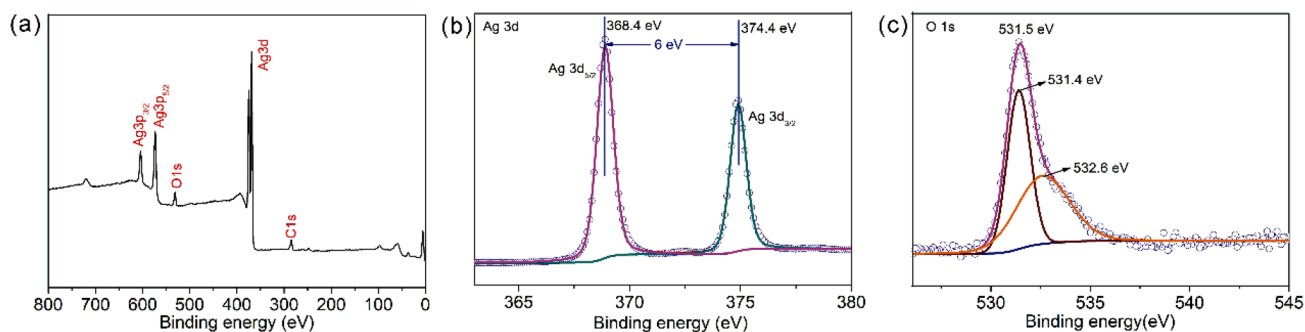

Fig. 8 XPS spectrum of the Ag NPs prepared at 520 V in 2 g L^{-1} Na$_2$SO$_4$ solution with 15 mL ethanol: **a** survey spectrum, **b** Ag 3d fine spectrum and **c** O 1s fine spectrum
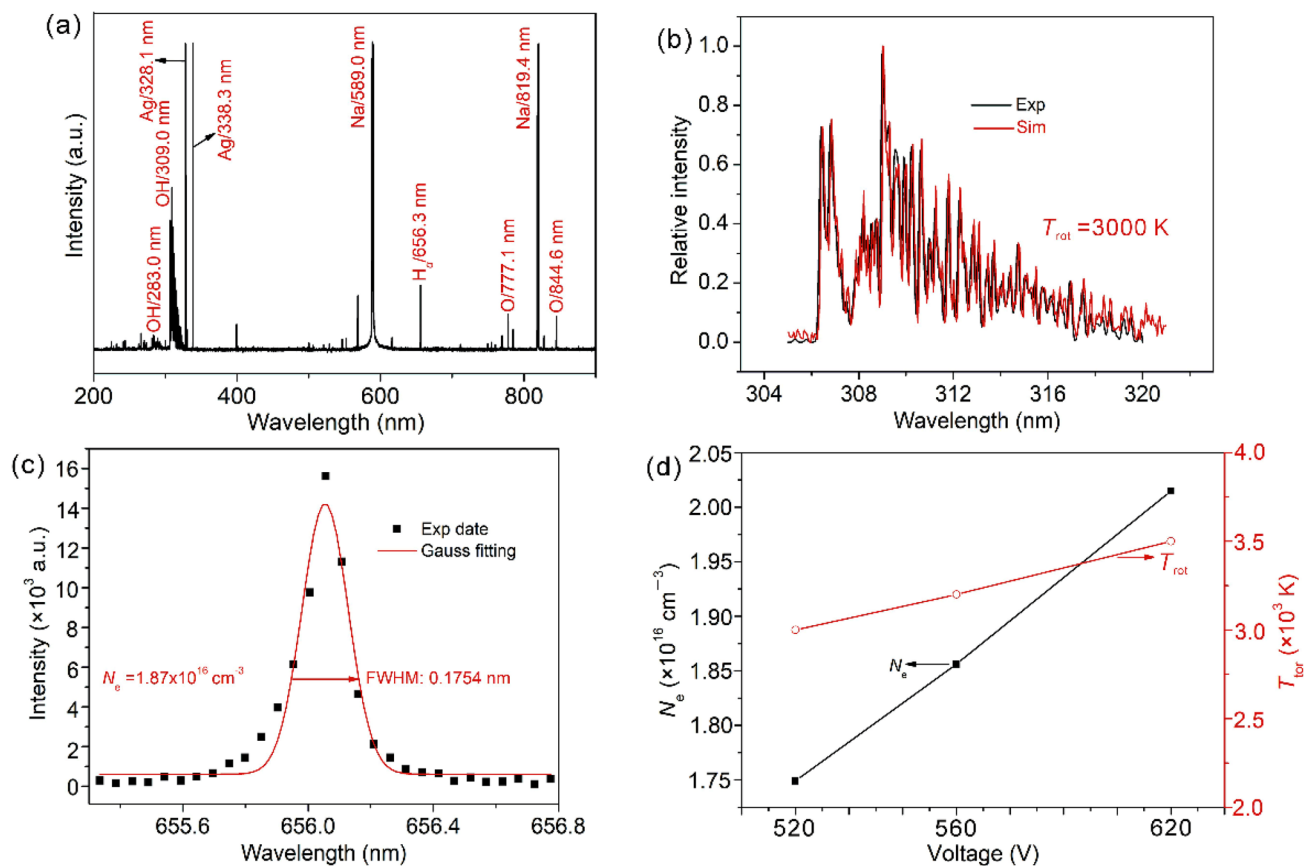
Fig. 9 **a** Optical emission spectra of the CGDE in 2 g L^{-1} Na$_2$SO$_4$ solution with adding 15 mL ethanol, **b** experimental and simulation curve of rotation temperature (T_{rot}), **c** Stark broadening profile and calculated electron density (N_e), **d** The change of rotation temperature (T_{rot}) and electron density (N_e) at different discharge voltage

with the simulated spectrum. Meanwhile, comparison of the simulated spectrum with the experiment repeatedly, until the best fitting spectrum is found. For example, Bruggeman et al. [60] reported the T_{rot} of OH is over 3250 K in the atmospheric pressure air discharges with a liquid cathode. Nomura et al. [61] found that the T_{rot} of OH in in-liquid plasma are over 3500. As illustrated in Fig. 9b, the T_{rot} at 520 V is about 3000 K. This result is basically consistent with the reported by Bruggeman et al. [60] and Nomura et al. [61].

The N_e is estimated using Stark-broadening of H$_\alpha$ (656.3 nm) [62, 63]:

$$N_e = 2.42 \times 10^{17} \left(\Delta\lambda_{1/2} \right)^{1.4713} \tag{2}$$

where, $\Delta\lambda_{1/2}$ is the full width at half maximum (FWHM) of the Stark broadening profile at H$_\alpha$ (656.3 nm) line. Figure 9c showed the H$_\alpha$ 656.3 nm line of the experimental and theoretical simulation curve of Gauss fitting. As presented in Fig. 9c, the FWHM is 0.1754 nm. Based on the Eq. (2), the N_e is 1.87×10^{16} cm^{-3} at 520 V.

Figure 9d shows the change of T_{rot} and N_e at different discharge voltage. As shown the Fig. 9d, the T_{rot} and N_e are increased with increasing the discharge voltage. That is, when the voltage increases from 520 to 620 V, the T_{rot} increases from 3000 to 3500 K, and the electron density increases from 1.87×10^{16} cm^{-3} to 2.01×10^{16} cm^{-3}. This is because the increase of discharge voltage can improve the discharge power and increase the electron number density, which increase the rotation temperature of OH, and lead to more atoms transition to the excited state, thus increasing the spectral line intensity, the excitation and ionization of water molecules and the number of electrons transition from high energy level to low energy level, and ultimately resulting in the production of more electrons [62].

Identification of acidity and/or basicity around the electrodes

To investigate the plasma effect, two glass tubes were also employed to separate the anodic and cathodic regions. The acidity and/or basicity of solution surrounding the

electrodes (Pt needle as cathode and Ag foil as anode) are identified by dropping indicator, such as methyl orange and phenolphthalein. The phenomenon in glass tubes are presented in Fig. 10a. The solution around Pt needle appears purple after dropping the phenolphthalein, and the solution around Ag foil presents red after dropping the methyl orange. The results indicated that under CGDE, anode and cathode are generated H^+ and OH^-, respectively.
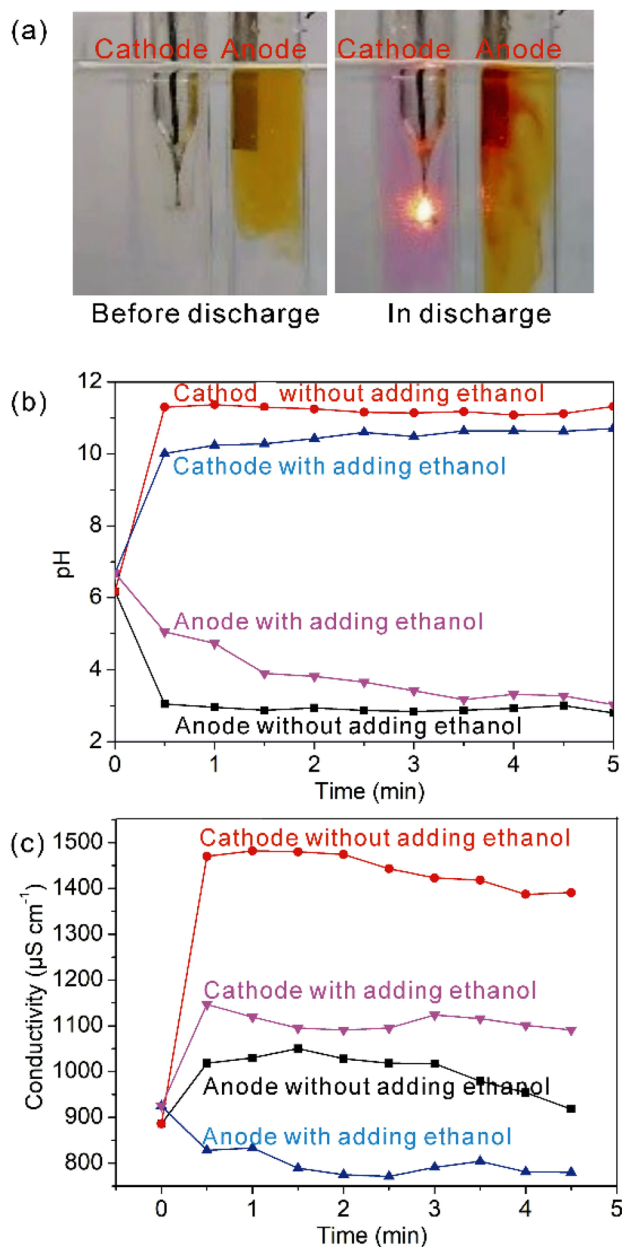

Fig. 10 **a** Verification of acidity and basicity around the electrodes before and during the process of discharge, **b** the pH change of anolyte and catholyte at different plasma treatment time, and **c** the conductivity change of anolyte and catholyte at different plasma treatment time

The pH and conductivity of cathode and anode solution at different treatment time

In order to further confirm the alkalinity and/or acidity, the pH values of catholyte and anolyte at different plasma treatment time were determined by a pH meter. As can be seen from Fig. 10b, the solution is almost neutral and its initial pH is about 6.3 before discharge. Without adding the ethanol, the pH value of anolyte solution is decreased to about 3.0 from pH = 6.3 (a), and catholyte solution gradually is increased to about 11.3 (b). These results imply that water loses electrons in anode to produce hydrogen ions, and high energetic electron irradiates the solution surface in cathode to generate OH^- [11, 19]. After adding the ethanol, the pH of the anode solution is decreased from the initial value of 6.3 to 3.2, and the pH of the cathode solution is increased from the initial value of 6.3 to 10.5. Compared with no adding the ethanol, the pH value of anolyte solution is increased and catholyte is decreased. This is because in the process of CGDE, ethanol can be oxidized to form acetic acid which cause the decrease of catholyte pH [64]. It is found (Fig. 10c) that the solution conductivity at anode has a slight increase, while at the plasma cathode rapidly increases to 1460 uS cm^{-1} in 30 s, suggesting that charged particles produced around cathode discharge are more than that of anode. After adding ethanol, the solution conductivity of anolyte and catholyte are all reduced compared with no ethanol at different treatment time, indicating that ethanol should participate in chemical reactions.

Measurement of solution pH and conductivity

To thoroughly understand the formation mechanism, the solution pH values and conductivity prepared Ag NPs before and after adding ethanol at different discharge times were also measured. As presented in Fig. 11a, the pH value of the solution without adding ethanol increases from 7.0 to 10.2 in about 5 min, then, it basically keeps a constant at approximately pH = 10.2. However, after adding ethanol, the pH value of the solution increases to about 9.0, then, remains a constant at about pH = 9.2, suggesting that adding ethanol can reduce the solution pH due to generate organic acid. In addition, after adding ethanol, the solution conductivity is reduced (Fig. 11b) because of forming the weak organic acid, i.e., acetic acid. In short, the preparation of Ag NPs is carried out under weak alkaline environment.

Proposed formation mechanism

The possible preparation mechanism of Ag NPs using CGDE was illustrated in Fig. 12. The process for the formation of Ag NPs involves five steps, which were described below:
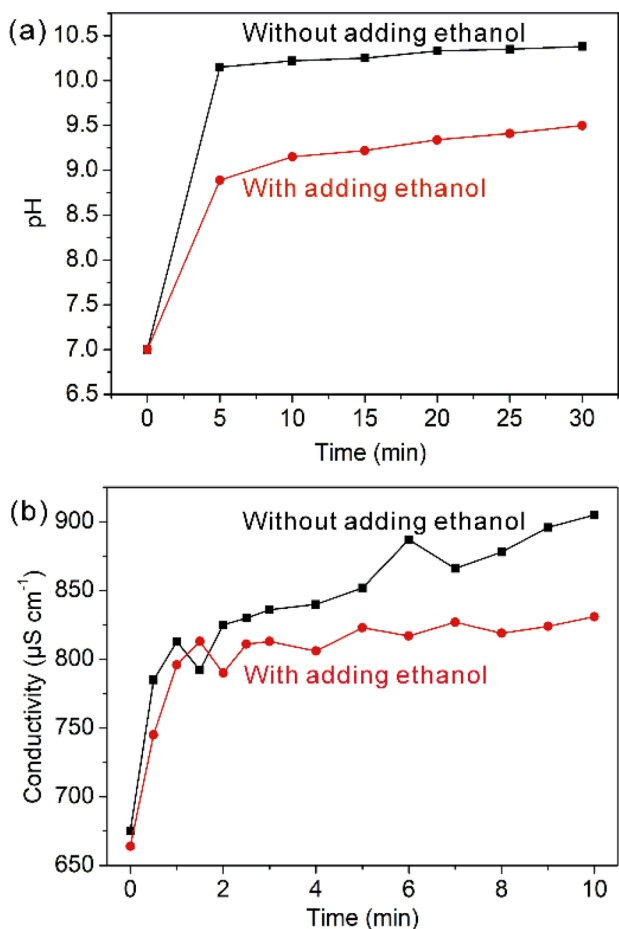
Fig. 11 Changes of **a** solution pH and **b** conductivity during the process of Ag NPs preparation at 520 V in 2 g L^{-1} Na$_2$SO$_4$ solution

1. Production of Ag$^+$ ions and release of the oxygen gas on the anode. In the anode, normal electrolysis occurs, and oxidation reactions lead to dissolution of the Ag foil into Ag$^+$ ions solution (reaction 3) [19].

   The anode:

$$Ag - e^{-\infty} \rightarrow Ag^+ \tag{3}$$

   Meanwhile, the anode is generated H$^+$ ions which result in the acidity and decrease the pH due to going through the reaction (4).
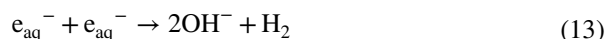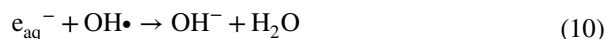
$$2H_2O - 4e^- \rightarrow 4H^+ + O_2 \tag{4}$$
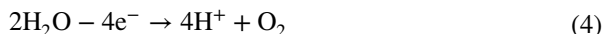
2. Generation of active species at cathode. In the cathode, at the plasma–liquid interface, the high energetic electrons (e*) produced by the solution plasma can decompose water and lead to the generation of active species such as H•, O•, OH• and e$_{aq}^-$ [45].
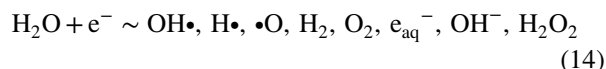
   At the plasma-liquid interface:

$$e^* + H_2O \rightarrow OH \bullet + H \bullet + e_{aq}^- \tag{5}$$

$$e^* + H_2O \rightarrow H \bullet + O \bullet + e_{aq}^- \tag{6}$$
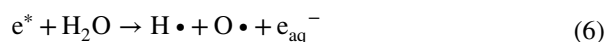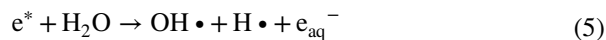
Then, these active species occur second-order recombination reactions [11, 45]:

$$OH \bullet + OH\bullet \rightarrow H_2O_2 \tag{7}$$

$$H \bullet + H\bullet \rightarrow H_2 \tag{8}$$

$$\bullet O + \bullet O \rightarrow O_2 \tag{9}$$

$$e_{aq}^- + OH\bullet \rightarrow OH^- + H_2O \tag{10}$$

$$e_{aq}^- + H\bullet \rightarrow OH^- + H_2 \tag{11}$$

$$e_{aq}^- + H_2O \rightarrow OH^- + H\bullet \tag{12}$$

$$e_{aq}^- + e_{aq}^- \rightarrow 2OH^- + H_2 \tag{13}$$

The total reaction at cathode is:

$$H_2O + e^- \sim OH\bullet, \ H\bullet, \ \bullet O, \ H_2, \ O_2, \ e_{aq}^-, \ OH^-, \ H_2O_2 \tag{14}$$

The yields of active species obtained at the glow discharge electrode are several times higher than that calculated from the Faradays' electrochemical law, which lead to high chemical reaction efficiency [26]. The catholyte is alkaline due to generation of OH$^-$ by energetic electron radiation (Reactions 10–13).

3. Formation of Ag/Ag$_2$O. In the solution, Ag$^+$ ions produced at anode migrate towards the plasma-liquid interface of cathode under the high electric field, and then occurs reduction reaction with e$_{aq}^-$ and H• generated in the process of CGDE to form Ag NPs around the cathode (Reactions 15 and 16) [64].

$$e_{aq}^- + Ag^+ \rightarrow Ag \tag{15}$$

$$H \bullet + Ag^+ \rightarrow Ag + H^+ \tag{16}$$

Meanwhile, Ag$^+$ ions can also react with OH$^-$ in catholyte to form AgOH white precipitate (Reaction 17). However, AgOH is unstable and rapidly converts to Ag$_2$O precipitate (Reaction 18) [64].

$$Ag^+ + OH^- \rightarrow AgOH \tag{17}$$

$$2AgOH \rightarrow Ag_2O + H_2O \tag{18}$$

Fig. 12 Preparation mechanism of Ag NPs by using CGDE at 520 V in 2 g L^{-1} Na$_2$SO$_4$ solution with adding 15 mL ethanol
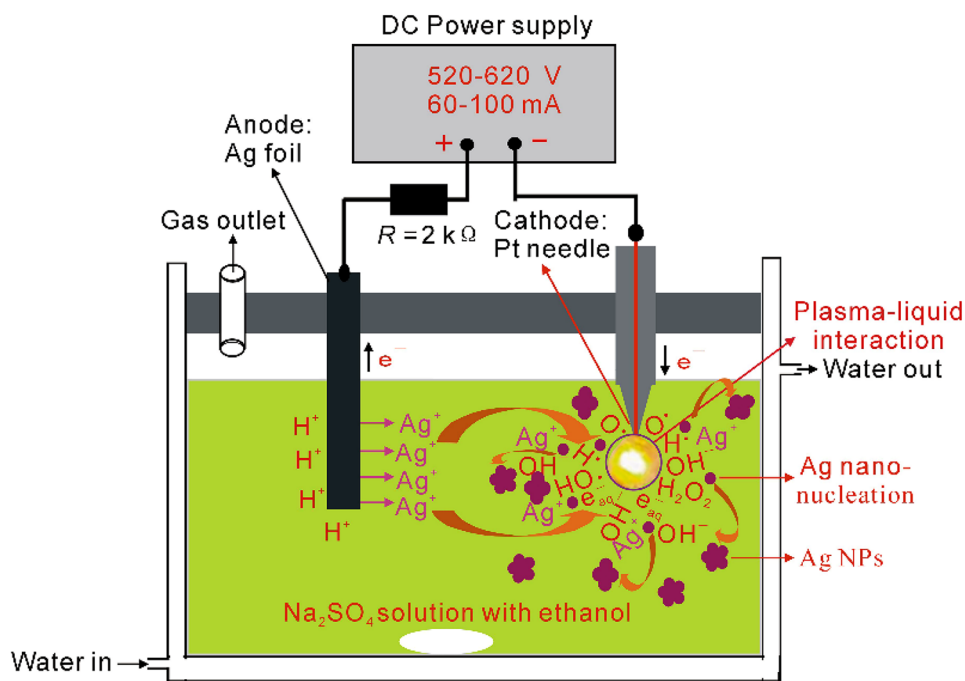

The solution color around cathode becomes grey, suggesting that Ag/Ag$_2$O mixed nanoparticles is formed. In addition, the color of the solution on the anode side does not change. The result indicated that the NPs are prepared at the interface between the cathode and the liquid by the energetic electron irradiation from the plasma. Moreover, from the spectral characteristics of CGDE, the Ag atomic lines appeared at 328.1 and 338.3 nm (Fig. 9a), indicating that Ag$^+$ ions are indeed moved into plasma cathode side. When the H$_2$O$_2$ generated by the plasma-liquid interactions is present in basic solutions (around cathode), the Ag$_2$O can react with H$_2$O$_2$ to form Ag [64].

$$Ag_2O + H_2O_2 \rightarrow 2Ag + H_2O + O_2 \tag{19}$$
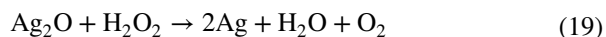
However, due to the low content of H$_2$O$_2$ and slow reaction rate, the produced Ag$_2$O particles are not entirely reduced to Ag NPs. Therefore, the nanoparticles with Ag and Ag$_2$O are formed without adding ethanol.

4. 4Forming pure Ag NPs with adding ethanol. Ethanol is known to trap OH• radicals to form acetaldehyde (CH$_3$CHO) and acetic acid (CH$_3$COOH). After adding ethanol, the reactions under CGDE are as follows [65]:

$$C_1H_5OH + OH\bullet \rightarrow H_2O + CH_3CHO \tag{20}$$

$$CH_3CHO + OH\bullet \rightarrow CH_3COOH \tag{21}$$
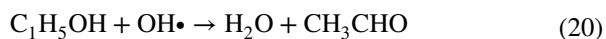
Meanwhile, CH$_3$CHO can also reduce Ag$_2$O/AgOH to form Ag in the alkaline solution. The reaction are as follows:

$$CH_3CHO + Ag_2O \rightarrow CH_3COOH + 2Ag \tag{22}$$

$$CH_3CHO + 2AgOH \rightarrow CH_3COOH + 2Ag + H_2O \tag{23}$$
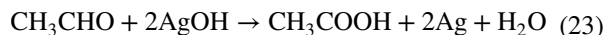
AgOH/Ag$_2$O and CH$_3$CHO occur redox reactions to produce CH$_3$COOH and Ag. The pH of catholyte is decreased due to forming CH$_3$COOH which reacts with OH$^-$. Therefore, Ag NPs were generated at the interface between the plasma cathode and the solution by CGDE using Ag$^+$ with adding ethanol. It is demonstrated that the role of ethanol is to suppress the generation of AgOH/Ag$_2$O in solution [45]. That is to say, the control of oxidation and reduction in the solution is possible by changing the electrolysis composition.

5. Formation of Ag NPs. The synthesis of Ag NPs by CGDE is owing to the presence of large number of hydrated electron (e$_{aq}^-$) and hydrogen radical (H•) for reduction of Ag$^+$ ions to Ag^0. Ag^0 atoms are fast combined into nanoclusters (nucleation of nanoparticles) in plasma-liquid interfaces, subsequent crystal growth, agglomeration, dispersion and stabilization into the solution (Reaction 24) that results in formation of Ag nanoparticles [7]. Consequently, high dispersion and small size of Ag NPs are generally obtained by CGDE.
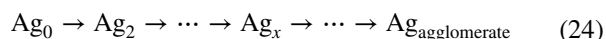
$$Ag_0 \rightarrow Ag_2 \rightarrow \cdots \rightarrow Ag_x \rightarrow \cdots \rightarrow Ag_{agglomerate} \tag{24}$$

Table 1 Conditions and characteristics of Ag NPs synthesized via plasma-liquid techniques

Method	Precursor	Stabilizer	Cathode	Anode	U (V)	t (min)	λ_{max} (nm)	Particle size (nm)	Ref.
Cathode glow discharge electrolysis	Na_2SO_4 with adding ethanol	/	Pt needle	Ag foil	520	30	441	20–80	This work
Solution plasma	$AgNO_3$	Alginate	W wire	W wire	800	7	415–440	5–40	[13]
Atmospheric pressure glow discharge	$AgNO_3$	D-fructose	W wire	Flowing liquid	1100–1300	/	404	14–16	[14]
Plasma-liquid electrolysis	HNO_3	Fructose	Ar plasma jet	Ag foil	2000	15	400	10	[15]
Dual He plasma electrolysis	$AgNO_3$	Sodium dodecyl sulfate (SDS)	He plasma jet	He plasma jet	/	2	400	/	[16]
He microplasma jet	$AgNO_3$	Sucrose	He plasma jet	Graphite rod	800	5	400	Below 11.2	[17]
Microplasma electrochemistry	$AgNO_3$	Fructose	He microplasma	Pt foil	2000	15	400	10–40	[18]
Ar microplasma jet	$AgNO_3$ solution	Dextran	Ar microplasma jet	Pt foil	400	20	396	16.5	[19]
Glow Discharge	$AgNO_3$	Glucose	Graphite rods	liquid anode	700	4	397	/	[20]
Contact glow discharge	NaOH, CH_3COONa, pH = 8	Polyvinyl pyrrolidone (PVP)	W wire	Ag plate	175–275	2	394–417	5–10	[21]
Microplasma glow discharge	$AgNO_3$, CH_3COONa, pH = 8	Sodium polyacrylate (NaPA)	W wire	Pt plate	250	0–15	410	2–20	[22]

The quantities of e_{aq}^- and H• are proportional to the particle charges. At low discharge, Ag^0 is produced at a slow rate which can grow and form into spherical shape Ag NPs due to a little bit of e_{aq}^- and H• produced by CGDE. When the discharge voltage increases, the increment of electrons and electric energy can result in forming many e_{aq}^- and H•. As a result, a reduction in Ag ions is able to occur quite quickly, which cause agglomeration of Ag NPs [39, 66]. According to the dedicated effort, the size distribution and particle size of Ag NPs can be tuned by manipulating the nucleation and growth rate through controlling discharge voltage and addition of ethanol as OH• scavengers [21].

Comparison of microplasma methods for the preparation of Ag NPs

A comparison of CGDE with other plasma-liquid interaction techniques for the preparation of Ag NPs was summarized in Table 1 [13–22]. As shown in Table 1, some plasma-liquid techniques are carried out in the inert gas (i.e. He or Ar) atmosphere [15–19]. In addition, electrolyte solution containing stabilizers and/or surfactants and the soluble silver salts (i.e., $AgNO_3$) are used as a precursor of Ag NPs [13, 14, 16–20, 22]. The use of silver salts makes difficult the

control of nanoparticles formation process from size and shape due to the gradual decrease of Ag^+ ions concentration in the working solution with the passing of discharge time [21]. Furthermore, some techniques required complex device [12, 14], accuracy control for parameters (i.e., ratios for the precursors and surfactants, solution pH, temperature) [21, 22], higher discharge voltage [14, 15, 18], and different large-scale production [15–20]. Compared with other synthesis methods, the CGDE by sacrificial anodes Ag foil offers some advantages, such as simple equipment, no inert gas consumption, no silver salt and surfactants, no secondary pollution, ease controlling reaction, and easy large-scale production. Therefore, it is a novel green technology for the preparation of Ag NPs. However, as presented in Table 1, the particle size of Ag NPs prepared via CGDE is bigger than those reported for other method. In future, reducing size and adjusting morphology will be the main research orientation.

Conclusion

Ag NPs were successfully prepared by one-step method via cathode glow discharge electrolysis plasma, in which Ag foil and Pt needle point were acted as anode and cathode, respectively. The main conclusions are as follows:

1. The optimal conditions for the preparation of Ag NPs are 150 mL 2 g L^{-1} Na_2SO_4 with adding 15 mL ethanol as electrolyte and 520 V applied voltage.

2. Adding ethanol into the liquid can trap oxidizing agent (OH•) and suppress producing $AgOH/Ag_2O$.

3. During the process of CGDE, the emission lines such as OH, H, O, Ag and Na are all observed. The T_{rot} increases from 3000 to 3500 K, and the electron density increases from 1.87×10^{16} cm^{-3} to 2.01×10^{16} cm^{-3}.

4. The pH of the anode solution decreases from the initial value of 6.3 to 3.2, and the pH of the cathode solution increases from the initial value of 6.3 to 10.5. Ag NPs were synthesized at solution pH = 9.2 via the reduction of Ag^+ ions by e_{aq}^- or H• at plasma cathode.

Compared with other plasma-liquid interface technique, GDEP offers some advantages such as simple equipment, no inert gas consumption, ease controlling the size of the product, and easy large-scale production. It is a new generation green technology for preparation of nanomaterials. Future work will further tune the size of obtained Ag NPs by changing experimental parameters, investigate the performance of prepared Ag NPs and extend the fabrication range of nanomaterials using CGDE.

Data availability The data that support the findings of this study are available from the corresponding author, upon reasonable request.

Declarations

Ethical approval This declaration is "not applicable".

Competing interests The authors declare no competing interests.

References

1. Behzad F, Naghib SM, Jadidikouhbanani MA, Tabatabaei SN, Zare Y, Rhee KY (2021) An overview of the plant-mediated green synthesis of noble metal nanoparticles for antibacterial applications. J Ind Eng Chem 94:92–104

2. Dzimitrowicz A, Bielawska-Pohl A, Cenzo GC, Jamroz P, Macioszczyk J, Klimczak A, Pohl P (2018) Pulse-modulated radio-frequency alternating-current-driven atmospheric- pressure glow discharge for continuous-flow synthesis of silver nanoparticles and evaluation of their cytotoxicity toward human melanoma cells. Nanomaterials 8:398

3. Sirotkin NA, Gurina DL, Khlyustova AV, Costerin DY, Naumova IK, Titov VA, Agafonov AV (2021) Experimental and computational investigation of polylactic acid/silver-NP nanocomposite with antimicrobial activity prepared by plasma in liquid. Plasma Process Polym 18:e2000169

4. Srikar SK, Giri DD, Pal DB, Mishra PK, Upadhyay SN (2016) Green synthesis of silver nanoparticles: A review. Green Sustainable Chem 6:34–56

5. Zhang Z, Shen WF, Xue J, Liu YM, Liu YW, Yan PP, Liu JX, Tang JG (2018) Recent advances in synthetic methods and applications of silver nanostructures. Nanoscale Res Lett 13:54

6. Yaqoob AA, Umar K, Ibrahim MNM (2020) Silver nanoparticles: various methods of synthesis, size affecting factors and their potential applications–A review. Appl Nanosci 10:1369–1378

7. Di LB, Zhang JS, Zhang XL (2018) A review on the recent progress, challenges, and perspectives of atmospheric-pressure cold plasma for preparation of supported metal catalysts. Plasma Process Polym 15:e1700234

8. Chen Q, Li JS, Li YF (2015) A review of plasma-liquid interactions for nanomaterial synthesis. J Phys D Appl Phys 48:424005

9. Saito G, Akiyama T (2015) Nanomaterial synthesis using plasma generation in liquid. J Nanomater 2015:1–21

10. Dzimitrowicz A, Jamroz P, Pogoda D, Nyk M, Pohl P (2017) Direct current atmospheric pressure glow discharge generated between a pin-type solid cathode and a flowing liquid anode as a new tool for silver nanoparticles production. Plasma Process Polym 14:1600251

11. Tochikubo F, Shimokawa Y, Shirai N, Uchida S (2014) Chemical reactions in liquid induced by atmospheric-pressure dc glow discharge in contact with liquid. Jpn J Appl Phys 53:126201

12. Rumbach P, Go DB (2017) Perspectives on plasmas in contact with liquids for chemical processing and materials synthesis. Top Catal 60:799–811

13. Nam S, Ali DM, Kim J (2016) Characterization of alginate/silver nanobiocomposites synthesized by solution plasma process and their antimicrobial properties. J Nanomater 2016:1–9

14. Dzimitrowicz A, Motyka-Pomagruk A, Cyganowski P, Babinska W, Terefinko D, Jamroz P, Lojkowska E, Pohl P, Sledz W (2018) Antibacterial activity of fructose-stabilized silver nanoparticles produced by direct current atmospheric pressure glow discharge towards quarantine pests. Nanomaterials 8:751

15. Richmonds C, Sankaran RM (2008) Plasma-liquid electrochemistry: Rapid synthesis of colloidal metal nanoparticles bymicroplasma reduction of aqueous cations. Appl Phys Lett 93:131501

16. Shirai N, Uchida S, Tochikubo F (2014) Synthesis of metal nanoparticles by dual plasma electrolysis using atmospheric dc glow discharge in contact with liquid. Jpn J Appl Phys 53:046202

17. Thong YL, Chin OH, Ong BH, Huang NM (2016) Synthesis of silver nanoparticles prepared in aqueous solutions using helium dc microplasma jet. Jpn J Appl Phys 55:01AE19

18. Huang Z, Zhong XX, Lu Y, Li YS, Rider AE, Furman SA, Ostrikov K (2013) Plasmonic Ag nanoparticles via environment-benign atmospheric microplasma electrochemistry. Nanotechnology 24:095604

19. Wang RX, Zuo SS, Zhu WD, Wu S, Nian WF, Zhang J, Fang J (2014) Microplasma-assisted growth of colloidal silver nanoparticles for enhanced antibacterial activity. Plasma Process Polym 11:44–51

20. Khlyustova A, Sirotkin N, Kochkina N, Krayev A, Titov V, Agafonov A (2019) Deposition of silver nanostructures on polymer films by glow discharge. Plasma Chem Plasma Process 39:311–323

21. Kuntyi OI, Kytsya AR, Bondarenko AB, Mazur AS, Mertsalo IP, Bazylyak LI (2021) Microplasma synthesis of silver nanoparticles

in PVP solutions using sacrificial silver anodes. Colloid Polym Sci 299:855–863

22. Shepida M, Kuntyi O, Sukhatskiy Y, Mazur A, Sozanskyi M (2021) Microplasma synthesis of antibacterial active silver nanoparticles in sodium polyacrylate solutions. Bioinorg Chem Appl 2021:4465363

23. Kareem TA, Kaliani AA (2012) Glow discharge plasma electrolysis for nanoparticles synthesis. Ionics 18:315–327

24. Zheng BC, Wang KL, Shrestha M, Schuelke T, Fan QH (2019) Understanding the chemical reactions in cathodic plasma electrolysis. Plasma Sources Sci Technol 28:085016

25. Sen Gupta SK (2015) Contact glow discharge electrolysis: its origin, plasma diagnostics and non-faradaic chemical effects. Plasma Sources Sci Technol 24:063001

26. Sen Gupta SK, Singh R (2017) Cathodic contact glow discharge electrolysis: Its origin and non-faradaic chemical effects. Plasma Sources Sci Technol 26:015005

27. Bruggeman PJ, Kushne MJ, Locke BR (2016) Plasma-liquid interactions: A review and roadmap. Plasma Sources Sci Technol 25:053002

28. Foster JE (2017) Plasma-based water purification: Challenges and prospects for the future. Phys Plasmas 24:055501

29. Yan ZC, Chen L, Wang HL (2008) Hydrogen generation by glow discharge plasma electrolysis of ethanol solutions. J Phys D Appl Phys 41:155205

30. Friedrich JF, Mix R, Schulze RD (2008) New plasma techniques for polymer surface modifaction with monotype functional groups. Plasma Process Polym 5:407–423

31. Lu QF, Yu J, Gao JZ, Yang W, Li Y (2011) Glow-discharge electrolysis plasma induced synthesis of polyvinylpyrrolidone/acrylic acid hydrogel and its adsorption properties for heavy-metal ions. Plasma Process Polym 8:803–814

32. Lu QF, Yang SX, Sun DX, Zheng JD, Li Y, Yu J, Su MG (2016) Direct determination of Cu by liquid cathode glow discharge-atomic emission spectrometry. Spectrochim Acta B 125:136–139

33. Allagui A, Baranova EA, Wüthrich R (2013) Synthesis of Ni and Pt nanomaterials by cathodic contact glow discharge electrolysis in acidic and alkaline media. Electrochim Acta 93:137–142

34. Lu QF, Li JL, Wang B, Yu J, Ma XJ, Cui LJ, Feng Y (2022) Preparation of TiO$_2$ nanoparticles via cathode glow discharge electrolysis and its photocatalytic performance in the degradation of methylene blue. Plasma Process Polym 19:2100172

35. Yu J, Wang B, Lu QF, Xiao L, Ma XJ, Feng Y, Qian YH (2023) Cathode glow discharge electrolysis synthesis of flower-like β-Ni(OH)$_2$ microsphere for high-performance supercapacitor. Chem Eng J 453:139769

36. Shadrin SY, Belkin PN, Tambovskiy IV, Kusmanov SA (2020) Physical features of anodic plasma electrolytic carburising of low-carbon steels. Plasma Chem Plasma Process 40:549–570

37. Wang XY, Zhou MH, Jin XL (2012) Application of glow discharge plasma for wastewater treatment. Electrochim Acta 83:501–512

38. Toriyabe Y, Watanabe S, Yatsu S, Shibayama T, Mizuno T (2007) Controlled formation of metallic nanoballs during plasma electrolysis. Appl Phys Lett 91:041501

39. Saito G, Sakaguchi N (2015) Solution plasma synthesis of Si nanoparticles. Nanotechnology 26:235602

40. Saito G, Hosokai S, Tsubota M, Akiyama T (2012) Ripple formation on a nickel electrode during a glow discharge in a solution. Appl Phys Lett 100:181601

41. Akolkar R, Sankaran RM (2013) Charge transfer processes at the interface between plasmas and liquids. J Vacuum Sci Technol A 31:050811

42. Shirai N, Ichinose K, Uchida S, Tochikubo F (2011) Influence of liquid temperature on the characteristics of an atmospheric dc glow discharge using a liquid electrode with a miniature helium flow. Plasma Sources Sci Technol 20:034013

43. Mkhalid IA, Fierro JLG, Mohamed RM, Alshahri AA (2020) Visible light driven photooxidation of imazapyr herbicide over highly efficient mesoporous Ag/Ag$_2$O–TiO$_2$ p-n heterojunction photocatalysts. Ceram Int 46:25822–25832

44. Jin SH, Kim SM, Lee SY, Kim JW (2014) Synthesis and characterization of silver nanoparticles using a solution plasma process. J Nanosci Nanotechnol 14:8094–8097

45. Tochikubo F, Shirai N, Uchida S (2014) Liquid-phase reactions induced by atmospheric pressure glow discharge with liquid electrode. J Phys Conf Ser 565:012010

46. Wankhede YB, Kondawar SB, Thakare SR, More PS (2013) Synthesis and characterization of silver nanoparticles embedded in polyaniline nanocomposite. Adv Mat Lett 4:89–93

47. Shahjahan M, Rahman MH, Hossain MS, Khatun MA, Islam A, Begum MHA (2017) Synthesis and characterization of silver nanoparticles by sol-gel technique. Nanosci Nanometrol 3:34–39

48. Kassaee MZ, Akhavan A, Sheikh N, Sodagar A (2008) Antibacterial effects of a new dental acrylic resin containing silver nanoparticles. J App Polym Sci 110:1699–1703

49. Ghosh T, Chattopadhyay A, Mandal AC, Pramanik S, Kuiri PK (2020) Optical, structural, and antibacterial properties of biosynthesized Ag nanoparticles at room temperature using Azadirachta indica leaf extract. Chin J Phys 68:835–848

50. Chiang WH, Richmonds C, Sankaran RM (2010) Continuous-flow, atmospheric-pressure microplasmas: a versatile source for metal nanoparticle synthesis in the gas or liquid phase. Plasma Sources Sci Technol 19:034011

51. Misran H, Salim MA, Ramesh S (2018) Effect of Ag nanoparticles seeding on the properties of silica spheres. Ceram Int 44:5901–5908

52. Dzimitrowicz A, Motyka A, Jamroz P, Lojkowska E, Babinska W, Terefinko D, Pohl P, Sledz W (2018) Application of silver nanostructures synthesized by cold atmospheric pressure plasma for inactivation of bacterial phytopathogens from the genera Dickeya and Pectobacterium. Materials 11:331

53. Lopez-Salido I, Dong CL, Kim YD (2005) Ag nanoparticles on highly ordered pyrolytic graphite (HOPG) surfaces studied using STM and XPS. Surf Sci 588:6–18

54. Cong Y, Xia T, Zou M, Li ZN, Peng B, Guo DZ, Deng ZW (2014) Mussel-inspired polydopamine coating as a versatile platform for synthesizing polystyrene/Ag nanocomposite particles with enhanced antibacterial activities. J Mater Chem B 2:3450–3461

55. Ma L, Huang Y, Hou M, Xie Z, Zhang Z (2015) Ag nanorods coated with ultrathin TiO$_2$ shells as stable and recyclable SERS substrates. Sci Rep 5:15442

56. Dey D, Halder N, Misra KP, Chattopadhyay S, Jain SK, Bera P, Kumar N, Mukhopadhyay AK (2020) Systematic study on the effect of Ag doping in shaping the magnetic properties of sol-gel derived TiO$_2$ nanoparticles. Ceram Int 46:27832–27848

57. Greda K, Swiderski K, Jamroz P, Pohl P (2016) Flowing liquid anode atmospheric pressure glow discharge as an excitation source for optical emission spectrometry with the improved detectability of Ag, Cd, Hg, Pb, Tl, and Zn. Anal Chem 88:8812–8820

58. Yuan H, Yang DZ, Li X, Zhang L, Zhou XF, Wang WC, Xu Y (2019) A pulsed electrolyte cathode discharge used for metal element analysis by atomic emission spectrometry. Phys Plasmas 26:053505

59. Luque J, Crosley DR (1999) LIFBASE: Database and Spectral Simulation (Version 1.5). SRI International Report MP 99-009

60. Bruggeman P, Ribel E, Maslani A, Degroote J, Malesevic A, Rego R, Vierendeels J, Leys C (2008) Characteristics of atmospheric pressure air discharges with a liquid cathode and a metal anode. Plasma Sources Sci Technol 17:025012

61. Nomura S, Mukasa S, Toyota H, Miyake H, Yamashita H, Maehara T, Kawashima A, Abe F (2011) Characteristics of in-liquid plasma in water under higher pressure than atmospheric pressure. Plasma Sources Sci Technol 20:034012

62. Yu J, Zhang XM, Lu QF, Wang X, Sun DX, Wang YQ, Yang W (2017) Determination of calcium and zinc in gluconates oral solution and blood samples by liquid cathode glow discharge-atomic emission spectrometry. Talanta 175:150–157

63. Liu YJ, Sun B, Wang L, Wang DG (2012) Characteristics of light emission and radicals formed by contact glow discharge electrolysis of an aqueous solution. Plasma Chem Plasma Process 32:359–368

64. Wu HH, Liu ZY, Xu LS, Wang X, Chen Q, Ostrikov K (2021) The Ag^+ reduction process in a plasma electrochemical system tuned by the pH value. J Electrochem Soc 168:123508

65. Chen Q, Lin J, He X, Hu HL, Li JS, Xiong Q, Chen B, Song ZY, Liu H, Liu QH, Ostrikov K (2019) Ethanol-controlled peroxidation in liquid-anode discharges. J Phys D Appl Phys 52:425205

66. Ranji MS, Yang BLY, Julaihi MRM (2020) Manipulation of electrolyte concentration and cathode morphology to control the size of the carbon nanoparticles. IOP Conf Series Mater Sci Eng 943:012007